UNIVERSITI MALAYSIA PERLIS
International Journal of Nanoelectronics and Materials
IJNeaM
ISSN 1985-5761 | E-ISSN 2232-1535

Room temperature carbon dioxide gas sensor based on europium oxide with a Kapton film as a flexible substrate

Kuberahventhan Sanmugavelan [a], Siti Amaniah Mohd Chachuli [b] *, Mohd Hafiz Jali [a], Sulaiman Wadi Harun [c], and Siddharth Thokchom [d]

[a]Fakulti Teknologi dan Kejuruteraan Elektrik, Universiti Teknikal Malaysia Melaka, Hang Tuah Jaya, 76100 Durian Tunggal, Melaka, Malaysia
[b]Fakulti Teknologi dan Kejuruteraan Elektronik dan Komputer, Universiti Teknikal Malaysia Melaka, Hang Tuah Jaya, Durian Tunggal 76100, Melaka, Malaysia
[c]Department of Electrical Engineering, University of Malaya, 50603 Kuala Lumpur, Malaysia
[d]School of Technology, Assam Don Bosco University, Guwahati, Assam, 781017, India
∗Corresponding author. e-mail: sitiamaniah@utem.edu.my

Received 27 June 2024, Revised 19 November 2024, Accepted 19 December 2024

ABSTRACT

The present research explores the fabrication and characterisation of thick films of europium oxide (Eu_2O_3), produced by the screen-printing method onto a Kapton film as a flexible substrate, for carbon dioxide (CO_2) gas sensing at room temperature. Eu_2O_3 has been chosen as sensing material for CO_2 gas due to the unique electrical structure, great sensitivity, and stability, and this study investigates the capability of Eu_2O_3 as gas sensor to interact with various CO_2 concentrations at room temperature. The project aims to develop three Eu_2O_3 thick film sensors (Peu1, Peu2, and Peu3) using screen-printing method. Furthermore, the films gas-sensing characteristics are fully examined utilizing methods such as field emission scanning electron microscopy (FESEM), energy-dispersive X-ray (EDX) spectroscopy, X-ray diffraction (XRD) and Raman spectroscopy. The result obtained from the graph of the I-V measurements of three Eu_2O_3 gas sensors were linear. Peu3 produced the highest response value of 1.53 at concentration of 30 sccm of CO_2. Whereas Peu1 produced response value of 1.66 and 1.97 at concentration of 50 sccm and 70 sccm of CO_2 gas, respectively. In general, Peu1 responded the best to different CO_2 gas concentrations and had the least resistance which was 0.666 GΩ. Redox interactions between CO_2 and Eu^{3+} ions at the Eu_2O_3 surface cause this drop in resistance by increasing the concentration of charge carriers and enhancing the electrical conductivity of the sensor material. These discoveries highlight the tremendous potential of Eu_2O_3 as a sensing material for several industrial applications, including the detection of greenhouse gases.

Keywords: *Binder, Carbon dioxide gas, Europium oxide, Kapton film, Screen-printing, Thick film gas sensor*

1. INTRODUCTION

Anthropogenic activities have led to an ever-increasing concentration of carbon dioxide (CO_2) in the environment, which has become a notable ecological issue primarily because of its role in accelerating global warming [1]. Therefore, the development of efficient and reliable CO_2 gas sensors is essential for environment monitoring, indoor air quality monitoring, and automotive cabin air quality. Deforestation, industrial operations, and the burning of fossil fuels are the three primary sources of atmospheric CO_2 [2]. Coal, oil, and natural gas are examples of fossil fuels that when burned to produce energy emit large volumes of CO_2 into the atmosphere. Deforestation and industrial operations like cement manufacture and chemical manufacturing also contribute to CO_2 emissions by releasing stored carbon back into the atmosphere and creating CO_2 as a byproduct of chemical reactions [3].

Europium oxide (Eu_2O_3) is ideal for gas sensors because of its unique electrical and structural features, which allow it to detect and respond to the presence of certain gases [4], [5]. The presence of europium ions (Eu^{3+}) in the oxide structure generates oxygen vacancies, which serve as active sites for gas adsorption and catalytic processes and can alter the material's electrical conductivity when exposed to target gases [6]. In this context, Eu_2O_3 exhibits distinct characteristics and a high phase purity, resulting in a suitable material for gas sensors [7]. The excellent phase purity of Eu_2O_3 contributes significantly to the performance and reliability of gas sensors by providing constant and precise detection of target gases [8]. Europium oxide's remarkable phase purity stems from its crystalline structure and the perfect placement of europium ions inside the lattice [8]. Europium oxide's stable phase structure guarantees that the sensor response is constant over time, reducing drift and guaranteeing dependable gas detection capabilities [9].

A study reported the development of a Eu_2O_3-based hydrogen sensor that could detect hydrogen concentrations as low as 100 ppm with a response time of less than 10 seconds [6] and a Eu_2O_3-based carbon monoxide (CO) sensor exhibited a linear response to CO concentrations ranging from 10 to 1000 ppm, with a fast response time and good repeatability [10]. The development of an optical CO_2

sensor based on Eu_2O_3 and its use in observing a yeast fermentation process revealed CO_2 concentration values that were comparable to those of a calibrated commercial CO_2 probe, confirming the calibration curve of the sensor and its suitability for real-world applications [11]. The researchers attributed the sensor's performance to the unique electronic structure and redox properties of Eu_2O_3. Additionally, it can be observed that when Eu_2O_3 thick films were exposed to CO_2 gas, the sensor resistance drastically reduced [12]. The alteration in resistance is ascribed to the redox processes that occur between CO_2 and Eu^{3+} ions at the surface of Eu_2O_3, therefore modulating the concentration of charge carriers and improving electrical conductivity [13]. The degree of the resistance change corresponds well with CO_2 concentration, allowing for excellent sensitive CO_2 detection.

The development of Eu_2O_3-based gas sensors represents prospective advances in gas sensing technology, particularly for CO_2 detection. Eu_2O_3 sensors outperform typical CO_2 sensors in terms of sensitivity, reaction time, and operating conditions, including those based on nanomaterials such as NiO-In_2O_3 nanospheres and lanthanum oxide (La_2O_3). Sensors based on NiO-In_2O_3 nanospheres, for example, have a sensitivity of 40% at 50 ppm CO_2 and a response time of 6 seconds at room temperature, whereas La_2O_3-based sensors have similar sensitivity and response characteristics but can be stable for up to 50 days [14, 15]. Furthermore, additional CO_2 sensors that rely on materials such as ZnO nanoflakes have demonstrated remarkable ultrafast response times of under 20 seconds; nevertheless, they necessitate high operating temperatures of 250°C [16]. The Eu_2O_3 sensors stand out due to their balance of high sensitivity, rapid response, and ability to work in ambient circumstances, making them a highly effective and novel solution for real time gas detection.

This study investigates the fabrication and characterisation of Eu_2O_3 thick films using a screen-printing technique for room temperature CO_2 sensing. Screen-printing is a low-cost and adaptable technology to fabricate thick film gas sensors, making it suitable for large-scale production and practical applications. Energy-Dispersive X-ray spectroscopy (EDX), Raman spectroscopy, Field Outflow Filtering Electron Microscopy (FESEM), and X-ray diffraction (XRD), were used in the characterisation of the fabricated thick films. The research involves the relationship between three thick films of Eu_2O_3 gas sensors for analysing the performance parameters of the suggested sensors toward different CO_2 concentrations at room temperature.

2. METHODOLOGY

2.1. Fabrication of Eu_2O_3 Thick Film Gas Sensor by Screen-Printed Method

A thick film gas sensor was constructed based on two layers: a thick film paste and an interdigitated electrode. To make a thick film paste, a binder should be mixed with a sensing material. Firstly, a binder was prepared by mixing 9.5 g of terpineol with 0.5 g of ethyl cellulose. The mixture was then agitated for 24 hours at 40°C and 200 rpm until it was mutually homogenous. Next, the sensing material was prepared by mixing 1 g of Eu_2O_3 with 1.4286 g of organic binder to make a paste. This specific agitation method was chosen to achieve thorough dissolution and uniform dispersion of the components. The temperature of 40°C reduces viscosity, which aids the blending process, while 200 rpm provides enough shear to enhance mixing. The 24 hours duration ensures that everything integrates well for optimal outcomes. This procedure was adapted from prior study [17]. After that, the mixture was agitated for three hours at 30°C and 80 rpm which led to the creation of Eu_2O_3 paste. The selection of 3 hours of agitation at 30°C and 80 rpm was chosen to ensure the thick film paste was not agglomerated during the mixing process and produced homogeneous paste to provide smooth surfaces of the sensing surface of the gas sensor during screen-printing fabrication. An interdigitated electrode was initially formed on a Kapton film and fired at 150°C for 30 minutes in an oven with a silver conductive paste. Next, the same screen-printing method was used to place a sensing film made entirely of Eu_2O_3 over the interdigitated electrode. After that, the constructed gas sensor was annealed for an hour at 200°C in an oven. Finally, a tiny copper wire coated with silver paste was joined to the leg of the interdigitated electrode, completing the gas sensor's electrical contact as shown in Figure 1. The three sensors Peu1, Peu2, and Peu3 were created using the same materials and methods with no major difference. However, slight differences in film thickness or surface texture due to the screen-printing process might impact their resistance values and sensing response to the carbon dioxide gas.

2.2. Characterisation of Eu_2O_3 Sensor

The structural, morphological, electrical, and gas sensing properties of the composites will be characterised by FESEM, XRD, and Raman spectroscopy. Field Emission Scanning Electron Microscopy (FESEM) reveals the uniform distribution of Eu_2O_3 particles within the thick films, forming a porous network structure that facilitates gas diffusion. The element composition and mapping of the carbon elements, oxygen, and Eu_2O_3 were analysed using an Energy Dispersive X-ray (EDX) within the FESEM to confirm the presence of Eu_2O_3 materials on the surface of the gas sensor. Raman spectroscopy range of 100 cm^{-1} to 1000 cm^{-1} aids in clarifying the Eu_2O_3 material's crystalline structure and vibrational modes. The XRD scan range for analysing Eu_2O_3 is between 20° and 80° to characterise demonstrated the high crystallinity and phase purity of the Eu_2O_3 material.

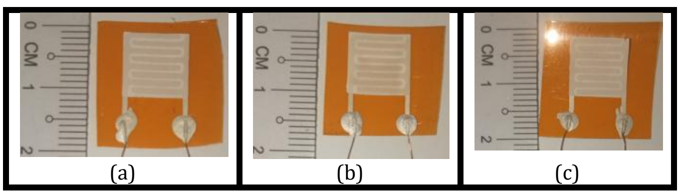

Figure 1. Eu_2O_3 Sensor (a) Peu1, (b) Peu2, and (c) Peu3

2.3. Experimental Setup of Eu_2O_3 Gas Sensors Toward Different Concentration CO_2 Gas

The experimental setup for the gas sensor was based on a schematic diagram of the gas chamber, as shown in Figure 2. First, the gas sensors were exposed to the flow of nitrogen gas acting as carrier gas followed by CO_2 concentrations which ranged from 30 sccm, 50 sccm, and 70 sccm. Each cycle of CO_2 gas flowed for 600 seconds. Three Eu_2O_3 sensor on thick film was examined for its capacity to detect CO_2 at room temperature. Labview software was used to record the gas sensor's response.

3. RESULTS AND DISCUSSION

3.1. Morphology of Eu_2O_3 Using FESEM

The surface morphology and microstructural characteristics of the Eu_2O_3 powder were revealed by the FESEM analysis at magnifications (10k) based on Figure 3 and Eu_2O_3 thick film FESEM analysis at magnifications (5k) based on Figure 4. Both investigations confirmed that the pure Europium Oxide's surface morphology and microstructural characteristics were quite similar even after fabrication, as demonstrated by the FESEM analysis referring to Figures 3 and 4. The finding reveals a rather homogenous microstructure with a dense and uniform crystalline structure of Eu_2O_3 nanoparticles throughout the film surface [18]. A high surface area-to-volume ratio is provided by the dense and homogeneous crystalline structure of Eu_2O_3 nanoparticles, which was essential for gas adsorption and interaction with gas molecules [19]. The uniform dispersion of nanoparticles enables constant gas adsorption sites, which leads to efficient gas detection.

3.2. EDX Analysis

Carbon, oxygen, and Eu_2O_3 were found to be the main constituents in the Eu_2O_3 thick film, as validated by the EDX

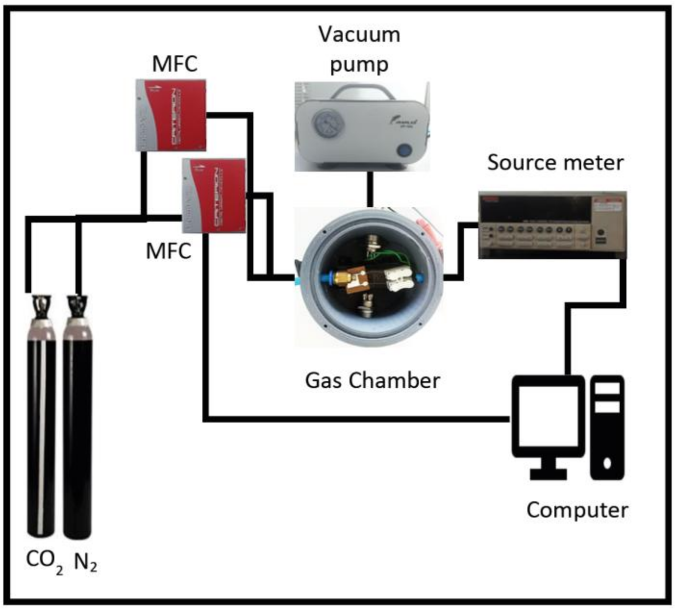

Figure 2. Gas Sensor Setup

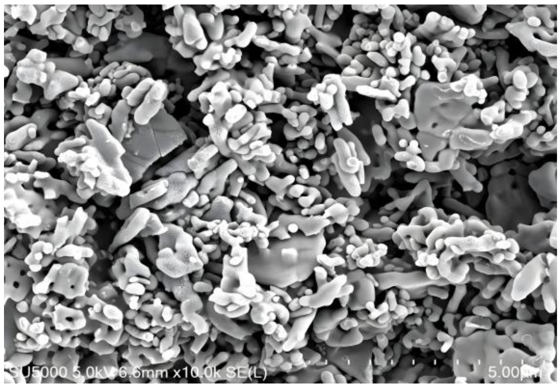

Figure 3. The Eu_2O_3 Powder using FESEM Analysis at Magnifications 10k

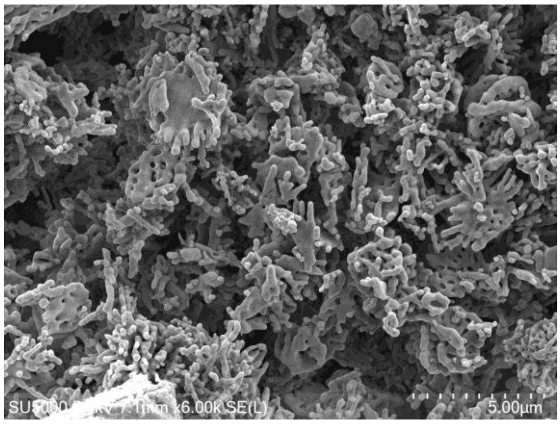

Figure 4. The Eu_2O_3 Thick Film using FESEM Analysis at Magnifications 5k

analysis based on Figure 5. The sample's weight percentage of Eu_2O_3 is 64.2%, as shown in data Table 1 and Figure 5. The exceptional purity of the material under investigation for gas sensing applications was confirmed by the high proportion of Eu_2O_3. Comprehending the charge transfer and resistance change processes during the gas sensing operation necessitates a comprehension of the existence of these constituents and their respective proportions [20].

Table 1. EDX analysis of Eu_2O_3 thick film

Elements	Weight (%)	Atomic (%)
Carbon	18.5%	50.7%
Oxygen	17.2%	35.4%
Europium oxide	64.2%	13.9%

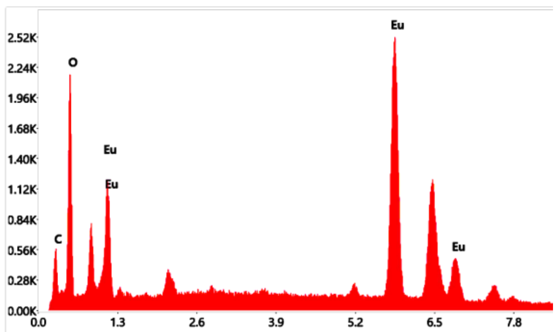

Figure 5. EDX analysis of Eu_2O_3 thick film

3.3. Raman Spectroscopy Analysis

The Eu_2O_3 Raman spectroscopy analysis structure's two-photon scattering process is responsible for the highest peak at 343.95 cm^{-1} followed by three major peaks at 784.91 cm^{-1}, 788.40 cm^{-1} and 777.01 cm^{-1} as displayed at Figure 6. This value reveals a similar peak at about 339.4 cm^{-1}, and it is in close agreement with the value provided in the linked study Eu_2O_3 nanocrystals synthesised using Aspalathus linearis extract [20]. The phase purity and crystallinity of the material synthesised in the current work are confirmed by the near match in the Raman shift values, which also validates the structural similarities of the Eu_2O_3 nanocrystals studied in this research. This peak results from the combination of two vibrational model. This mode is connected to the Eu–O bonds in the Eu_2O_3 structure's asymmetric stretching. The existence and strength of this peak provide illumination regarding the thick film sample's structural integrity and further support the cubic phase's genesis [21].

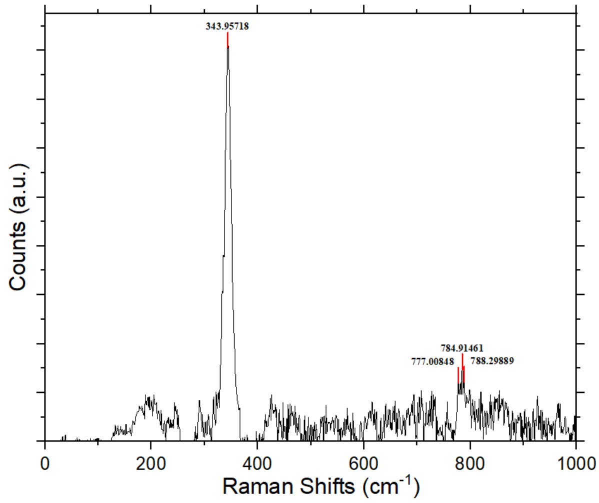

Figure 6. Raman spectroscopy analysis of Eu_2O_3

3.4. XRD Analysis

Figure 7 displays XRD analysis of Eu_2O_3 thick film. The apparent peaks observed in the XRD analysis include the (211), (321), (111), (220), (400), (511), (611), (612), and (421) planes. The highest peaks at 38.19°, are associated with the cubic fluorite structure of Eu_2O_3, which correspond to the (311) plane as presented in Ref. [22]. This result indicates that the expected Eu_2O_3 phase was crystalline since the peaks produced were near to the peaks as discussed in [22]. A thorough investigation of peak broadening is required for an accurate assessment of crystallite size. Peak intensities vary, most likely because of the crystal structure and the sample's crystallites' preferred orientation [23]. Certain crystallographic planes refract X-rays more effectively than others, resulting in discrepancies in measured intensities [24].

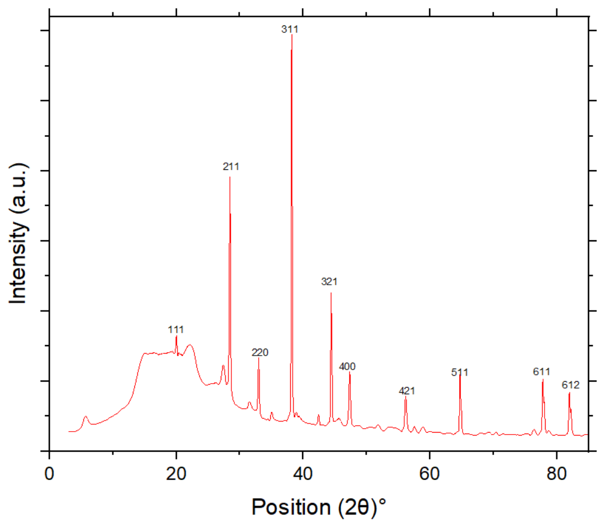

Figure 7. XRD analysis of Eu_2O_3 thick film

3.5. The Performance Parameters of Eu_2O_3 Sensors Toward Different CO_2 Concentrations at Room Temperature

The resistance of Eu_2O_3 gas sensors of Peu1, Peu2, and Peu3 were approximately 0.666 GΩ, 0.695 GΩ, and 0.690 GΩ, respectively which can be obtained by referring to Equation (1) from I-V measurement graph of these three Eu_2O_3 gas sensors based on Figure 8. The result obtained from the graph of the I-V measurement of three Eu_2O_3 gas sensors was linear. The measurement of Eu_2O_3 in terms of electrical characteristics is connected to Ohm's Law, in which the current flowing through a conductor is directly proportional to the voltage applied across it at a constant temperature [25]. The characteristics of Ohm's Law are observed in the conductivity behaviour, resistance, and reaction of Eu_2O_3 to changing voltages and currents during the measuring procedure. The resistance of the gas sensor can be calculated using the formula as follows:

$$R = \frac{1}{Slope} \tag{1}$$

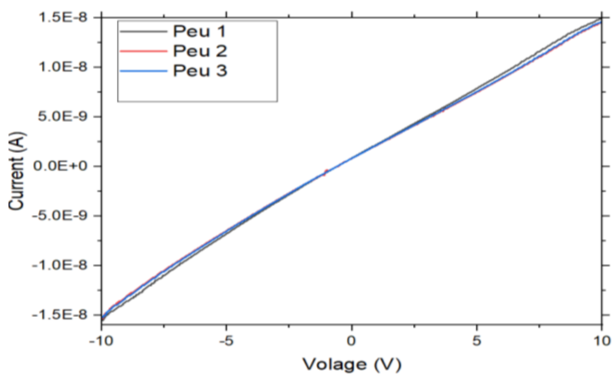

Figure 8. I-V measurement of three Eu_2O_3 gas sensor

Figure 9 presents the graph of three Eu_2O_3 gas sensor performances towards CO_2 at room temperatures. Then the sensing response of the gas sensors towards CO_2 which can be obtained by referring to Equation (2) was tabulated in Table 2 based on Figure 9. Peu3 showed highest response of the gas sensors towards 30 sccm concentration of CO_2 gas which was 1.53. However, Peu1 showed the highest response than other gas sensors at CO_2 concentration of

Table 2. Response of three Eu_2O_3 gas sensors toward different concentrations of CO_2 gas

Gas Sensor	Response of Sensors Toward CO_2 Gas		
	30 sccm	50 sccm	70 sccm
Peu1	1.36	1.66	1.97
Peu2	1.12	1.32	1.62
Peu3	1.53	1.35	1.38

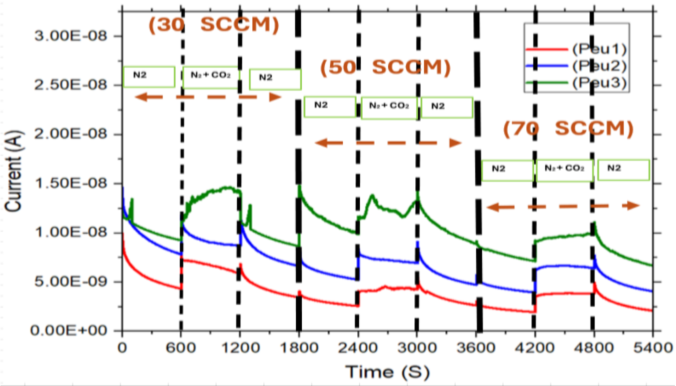

Figure 9. Three Eu_2O_3 gas sensor performances towards CO_2 gas under room temperatures

50 sccm and 70 sccm c which were 1.66 and 1.97, respectively. The sensing response of the gas sensor was defined as follows [26]:

$$s = \frac{I_{CO_2}}{I_{N_2}} \tag{2}$$

where I_{CO2} is current during CO_2 gas at saturated value and I_{N2} is current during nitrogen exposure at saturated value.

Peu1 shows the best response and performance towards different concentrations of CO_2 at room temperatures and has the lowest resistance based on Figure 9 and Table 2 even though it has the second-best response in 30 sccm concentration of CO_2 gas only. The Eu^{3+} ions on the surface of the material interact with CO_2 molecules when the Eu_2O_3 thick film is exposed to CO_2 gas as in Figure 9. The redox process that results from this interaction converts CO_2 into CO_3^{2-} and reduces Eu^{3+} ions to Eu^{2+} ions [27]. The general response can be shown as follows:

$$2Eu^{3+} + CO_2 \rightleftharpoons 2\,Eu^{2+} + CO_3^{2-} \tag{3}$$

This redox process alters the concentration of charge carriers in the Eu_2O_3 film, resulting in a considerable drop in sensor resistance. The material's electrical conductivity is improved when Eu^{3+} is reduced to Eu^{2+} because there are more charge carriers in the substance [14]. The amount that the resistance changes is directly correlated with the CO_2 gas concentration. The redox reaction's extent grows with rising CO_2 concentration, which causes the sensor resistance to fall significantly [13]. The connection between sensor resistance and CO_2 concentration allows the Eu_2O_3 thick film to detect CO_2 gas with great sensitivity. When the resistance of Peu2 and Peu3 increases based on Figure 9 and Table 2, the sensor's performance was dropped upon exposure towards CO_2. The resistance of the film changes in response to the CO_2 interaction-induced change in electrical conductivity. A gas sensor with better sensitivity often demonstrates a larger change in resistance when exposed to the target gas [28]. Consequently, the n-type operating mode of the Eu_2O_3 sensor and the measuring configuration resistance increase assessed as a positive response determine the link between resistance change and sensor sensitivity. A less sensor response for an n-type Eu_2O_3 sensor is shown by a drop in conductivity resulting from an increase in resistance following CO_2 exposure [28]. On the other hand, a p-type Eu_2O_3 sensor's increased conductivity as a result of a decrease in resistance in response to CO_2 exposure would be seen as a positive reaction and suggestive of increased CO_2 [29]. Peu3 shows the least performance towards CO_2 when the concentration increases even though it has the second highest resistance. This was due to the minimal change in resistance for Peu3 signifies weak interaction with the target gases, leading to low performance as the concentration of CO_2 increases [30], [31]. This limited interaction leads to a reduced redox reaction, prohibiting efficient conversion of CO_2 into carbonate ions and reduction of Eu^{3+} ions to Eu^{2+} ions. As a result, fewer charge carriers are generated, resulting in minimal resistance changes and reduced sensitivity. Peu3 higher resistance does not compensate for its poor interaction with CO_2, resulting in poorer performance.

3.6. Comparison of Eu_2O_3 Sensors toward CO_2 Gas with Past Literature

Table 3 lists the characteristics of CO_2 gas using various sensing materials such as ZnO, La_2O_3, and In_2O_3 with our work. It can be observed that some of the sensing material

Table 3. Comparison of CO_2 sensor using various sensing materials

Sensing Material	CO_2 Level	Operating Temperature (°C)	Response Value (S)		Ref.
			$\frac{R_{gas}-R_{air}}{R_{air}}$ (%)	$\frac{I_{CO_2}}{I_{N_2}}$	
La_2O_3	200 ppm	410	120	1.17	[13]
rGO/NiO-In_2O_3	50 ppm	Room temperature	40	1.60	[14]
La_2O_3	50 ppm	Room temperature	80	1.03	[15]
ZnO	1000 ppm	250	-	2.00	[16]
Eu_2O_3	30 sccm 50 sccm 70 Sccm	Room temperature	60 90 88	1.53 1.66 1.97	This work

worked at high operating temperatures to sense low concentrations of CO_2 gas. It can be seen that Eu_2O_3 is a potential sensing material that can be used as CO_2 gas sensor at room operating temperatures. Even though the response value is not as high as other sensing materials, this Eu_2O_3 can be used to detect CO_2 gas, and the sensing response can be enhanced in future work by doping with other materials based on metal such as silver nanoparticles [32] and graphene nanoflakes [33]. Nanostructured or doped forms of Eu_2O_3 can improve sensitivity and decrease operating temperatures, making it more competitive for real-world applications.

4. CONCLUSION

This study explored the fabrication and characterisation of Eu_2O_3 thick films for CO_2 gas detection applications at room temperature using a screen-printing approach. Field Emission Scanning Electron Microscope (FESEM), Energy Dispersive X-ray (EDX), X-ray diffraction (XRD), and Raman spectroscopy results have been presented and verified. Briefly, Peu1 had the greatest response value at 50 and 70 sccm concentrations of CO_2 gas, as well as the least resistance, making it the most effective gas sensor, while Peu3 had the best response at 30 sccm concentrations of CO_2 gas only. A drop in Eu^{3+} to Eu^{2+} and a subsequent decrease in sensor resistance are caused by the interaction between CO_2 particles and Eu^{3+} particles on the film's surface, which is likely included in the detecting apparatus. In conclusion, this study demonstrates the possibility of screen-printed Eu_2O_3 thick films as an effective room temperature CO_2 gas detection method. In future work, the Eu_2O_3-based sensors will be doped with metal-based materials such as graphene with various weigh ratios to improve the sensing response to the CO_2 gas. The Eu_2O_3-based sensors may be developed for practical uses in natural observation and outflow control by exploring various fabric modifications and improving the manufacturing process.

ACKNOWLEDGMENTS

The authors would like to thank the Advanced Sensors & Embedded Control (ASECs) Research Group, Faculty of Electronics and Computer Technology and Engineering, Universiti Teknikal Malaysia Melaka for providing available resources in laboratory and financial assistance.

REFERENCES

[1] M. Redlin and T. Gries, "Anthropogenic climate change: the impact of the global carbon budget," *Theoretical and Applied Climatology*, vol. 146, no. 1–2, pp. 713–721, Oct. 2021, doi: 10.1007/s00704-021-03764-0.

[2] P. Friedlingstein *et al.*, "Global Carbon Budget 2020," *Earth System Science Data*, vol. 12, no. 4, pp. 3269–3340, Dec. 2020, doi: 10.5194/essd-12-3269-2020.

[3] D. Cui, Z. Deng, and Z. Liu, "China's non-fossil fuel CO_2 emissions from industrial processes," *Applied Energy*, vol. 254, p. 113537, Nov. 2019, doi: 10.1016/j.apenergy.2019.113537.

[4] P.-G. Su and N.-H. Choy, "Electrical and Humidity-Sensing Properties of $EuCl_2$, Eu_2O_3 and $EuCl_2/Eu_2O_3$ Blend Films," *Chemosensors*, vol. 9, no. 10, p. 288, Oct. 2021, doi: 10.3390/chemosensors9100288.

[5] T. Hyodo, Y. Takakura, K. Kuroiwa, K. Tsuchiya, and Y. Shimizu, "Basic Gas-Sensing Properties of Photoluminescent Eu_2O_3-Mixed SnO_2-Based Materials with Submicron-Size Macropores," *Journal of Nanoscience and Nanotechnology*, vol. 19, no. 8, pp. 5351–5360, Aug. 2019, doi: 10.1166/jnn.2019.16829.

[6] C. Lupan *et al.*, "Nanosensors Based on a Single ZnO:Eu Nanowire for Hydrogen Gas Sensing," *ACS Applied Materials & Interfaces*, vol. 14, no. 36, pp. 41196–41207, Sep. 2022, doi: 10.1021/acsami.2c10975.

[7] S. Cao, N. Sui, P. Zhang, T. Zhou, J. Tu, and T. Zhang, "TiO_2 nanostructures with different crystal phases for sensitive acetone gas sensors," *Journal of Colloid and Interface Science*, vol. 607, pp. 357–366, Feb. 2022, doi: 10.1016/j.jcis.2021.08.215.

[8] J. Łażewski *et al.*, "Lattice Dynamics and Structural Phase Transitions in Eu_2O_3," *Inorganic Chemistry*, vol. 60, no. 13, pp. 9571–9579, Jul. 2021, doi: 10.1021/acs.inorgchem.1c00708.

[9] R. Banda, F. Forte, B. Onghena, and K. Binnemans, "Yttrium and europium separation by solvent extraction with undiluted thiocyanate ionic liquids," *RSC Advances*, vol. 9, no. 9, pp. 4876–4883, 2019, doi: 10.1039/C8RA09797F.

[10] P. P. Ortega *et al.*, "Towards carbon monoxide sensors based on europium doped cerium dioxide," *Applied Surface Science*, vol. 464, pp. 692–699, Jan. 2019, doi: 10.1016/j.apsusc.2018.09.142.

[11] E. N. Benton, N. A. K. R. Perera, V. N. Nesterov, W. Perera, M. A. Omary, and S. B. Marpu, "A Europium-Based Optical Sensor for the Detection of Carbon Dioxide and Its Application for a Fermentation Reaction," *Chemosensors*, vol. 11, no. 1, p. 5, Dec. 2022, doi: 10.3390/chemosensors11010005.

[12] J. Zhu *et al.*, "Gallium Oxide for Gas Sensor Applications: A Comprehensive Review," *Materials*, vol. 15, no. 20, p. 7339, Oct. 2022, doi: 10.3390/ma15207339.

[13] M. Andreev *et al.*, "Flame-Made La_2O_3-Based Nanocomposite CO_2 Sensors as Perspective Part of GHG Monitoring System," *Sensors*, vol. 21, no. 21, p. 7297, Nov. 2021, doi: 10.3390/s21217297.

[14] M. Amarnath and K. Gurunathan, "Highly selective CO_2 gas sensor using stabilized NiO-In_2O_3 nanospheres coated reduced graphene oxide sensing electrodes at room temperature," *Journal of Alloys and Compounds*, vol. 857, p. 157584, Mar. 2021, doi: 10.1016/j.jallcom.2020.157584.

[15] A. Eswaran, M. Thirumalainambi, R. Subramaniam, and G. Annadurai, "Highly selective CO_2 sensing response of lanthanum oxide nanoparticle electrodes at ambient temperature," *Nanoscale Advances*, vol. 5, no. 14, pp. 3761–3770, 2023, doi: 10.1039/D3NA00199G.

[16] S. Kanaparthi and S. G. Singh, "Chemiresistive Sensor Based on Zinc Oxide Nanoflakes for CO_2 Detection," *ACS Applied Nano Materials*, vol. 2, no. 2, pp. 700–706, Feb. 2019, doi: 10.1021/acsanm.8b01763.

[17] S. A. Mohd Chachuli *et al.*, "Effects of silver diffusement on TiO_2-B_2O_3 nanocomposite sensor towards hydrogen sensing," *Materials Research Innovations*, vol. 28, no. 5, pp. 365–378, Jul. 2024, doi: 10.1080/14328917.2024.2304480.

[18] T. R. Poorani, C. Ramya, and M. Ramya, "Effect of Topo Ratio in the Formation of In-Situ Hydrophobic Core–Shell Nanoparticle of Europium Oxide," *Journal of Inorganic and Organometallic Polymers and Materials*, vol. 33, no. 11, pp. 3413–3440, Nov. 2023, doi: 10.1007/s10904-023-02779-6.

[19] P. G. Choi, T. Fuchigami, K. Kakimoto, and Y. Masuda, "Effect of Crystal Defect on Gas Sensing Properties of Co_3O_4 Nanoparticles," *ACS Sensors*, vol. 5, no. 6, pp. 1665–1673, Jun. 2020, doi: 10.1021/acssensors.0c00290.

[20] W. Liu *et al.*, "Charge transfer driven by redox dye molecules on graphene nanosheets for room-temperature gas sensing," *Nanoscale*, vol. 13, no. 44, pp. 18596–18607, 2021, doi: 10.1039/D1NR04641A.

[21] A. Diallo, B. M. Mothudi, E. Manikandan, and M. Maaza, "Luminescent Eu_2O_3 nanocrystals by *Aspalathus linearis* ' extract: structural and optical properties," *Journal of Nanophotonics*, vol. 10, no. 2, p. 026010, Apr. 2016, doi: 10.1117/1.JNP.10.026010.

[22] P. Kuppusamy, S. Kim, S.-J. Kim, M. Park, and K.-D. Song, "Synthesizing fluorescent europium oxide nanosheets for the detection of ampicillin using a photoluminescence-based assay," *Journal of Saudi Chemical Society*, vol. 28, no. 1, p. 101795, Jan. 2024, doi: 10.1016/j.jscs.2023.101795.

[23] J. N. Lalena, D. A. Cleary, and O. B. M. H. Duparc, *Principles of Inorganic Materials Design*. Wiley, 2020. doi: 10.1002/9781119486879.

[24] D. A. Yatsenko, V. P. Pakharukova, and S. v. Tsybulya, "Low Temperature Transitional Aluminas: Structure Specifics and Related X-ray Diffraction Features," *Crystals*, vol. 11, no. 6, p. 690, Jun. 2021, doi: 10.3390/cryst11060690.

[25] B. Guo *et al.*, "Single-Crystalline Metal Oxide Nanostructures Synthesized by Plasma-Enhanced Thermal Oxidation," *Nanomaterials*, vol. 9, no. 10, p. 1405, Oct. 2019, doi: 10.3390/nano9101405.

[26] S. Amaniah Mohd Chachuli, M. Nizar Hamidon, M. Ertugrul, Md. S. Mamat, H. Jaafar, and N. H. Shamsudin, "TiO_2/B_2O_3 thick film gas sensor for monitoring carbon monoxide at different operating temperatures," *Journal of Physics: Conference Series*, vol. 1432, no. 1, p. 012040, Jan. 2020, doi: 10.1088/1742-6596/1432/1/012040.

[27] Y. Zhai, J. Du, C. Chen, W. Li, and J. Hao, "The photoluminescence and piezoelectric properties of Eu_2O_3 doped KNN-based ceramics," *Journal of Alloys and Compounds*, vol. 829, p. 154518, Jul. 2020, doi: 10.1016/j.jallcom.2020.154518.

[28] H. Wang, Y. Yang, T. Xie, and Y. Lin, "Highly Sensitive and Selective HCHO Sensor Based on Co Doped ZnO Hollow Microspheres Activated by UV Light," *IEEE Sensors Journal*, vol. 21, no. 6, pp. 7558–7564, Mar. 2021, doi: 10.1109/JSEN.2021.3050164.

[29] A. A. Yadav, A. C. Lokhande, J. H. Kim, and C. D. Lokhande, "Enhanced sensitivity and selectivity of CO_2 gas sensor based on modified La_2O_3 nanorods," *Journal of Alloys and Compounds*, vol. 723, pp. 880–886, Nov. 2017, doi: 10.1016/j.jallcom.2017.06.223.

[30] S. Madhu, S. Ramasamy, and J. Choi, "Recent Developments in Electrochemical Sensors for the Detection of Antibiotic-Resistant Bacteria," *Pharmaceuticals*, vol. 15, no. 12, p. 1488, Nov. 2022, doi: 10.3390/ph15121488.

[31] N. D. M. Said, M. Z. Sahdan, N. Nayan, A. S. Bakri, N. A. Raship, H. Saim, K. M. Wibowo, F. Adriyanto, "Rapid Response Room Temperature Oxygen Sensor Based on Trivalent-Elements Doped TiO_2 Thin Film," *International Journal of Nanoelectronics & Materials*, vol. 14, no. 3, 2021.

[32] N. H. Shamsudin *et al.*, "Impact of polyvinylpyrrolidone and quantity of silver nitrate on silver nanoparticles sizing via solvothermal method for dye-sensitized solar cells," *Surface and Interface Analysis*, vol. 54, no. 2, pp. 109–116, Feb. 2022, doi: 10.1002/sia.7026.

[33] S. Amaniah Mohd Chachuli, M. Luqman Hakkim Noor, O. Coban, N. Hazahsha Shamsudin, and M. Idzdihar Idris, "Characteristic of graphene-based thick film gas sensor for ethanol and acetone vapor detection at room temperature," *Indonesian Journal of Electrical Engineering and Computer Science*, vol. 32, no. 3, p. 1384, Dec. 2023, doi: 10.11591/ijeecs.v32.i3.pp1384-1391.